Influence of WC Addition on Microstructures of Laser-Melted Ni-Based Alloy Coating

Y.M. Zhang, M. Hida, A. Sakakibara, and Y. Takemoto

(Submitted 7 July 2001; in revised form 16 October 2001)

Nickel-based alloy powder was surface melted on S45C steel substrate using a CO2 laser. The effect of tungsten carbide (WC) on the interface layer and microstructures in the laser melted layer has been investigated by x-ray diffraction (XRD) analysis, and by scanning and transmission electron microscopy (SEM and TEM) techniques. There are three zones in the laser melted layer: the alloyed zone, the interface zone, and the heat affected zone of substrate. The interface zone appears as a smooth bright layer of single γ-(Fe, Ni) phase that serves as a primary crystallization phase in the laser alloyed zone. K-S lattice correspondence was recognized between γ-(Fe, Ni) in the interface and martensite in the substrate. The size of dendritic crystals decreased and eutectic structures in the laser alloyed layer changed after the addition of WC.

Keywords interface, laser-alloyed layer, NiCrBSi, transmission electron microscope, WC

1. Introduction

Laser surface alloying (LSA) is a novel method of producing high quality surface layers in components where the working conditions lead to highly abrasive wear.[1-5] The benefits of the LSA technique include reduction in the amount of alloying elements needed, refinement of grain size, extension of solid solubility of alloying elements, homogeneity of microstructures, metallurgical bonding but minimal damage to the substrate, and improvement in hardness.[6-12] The coating materials for the LSA are usually self-fluxing alloys based on NiCrBSi; in most cases, refractory carbides such as tungsten carbide (WC), vanadium carbide (VC), and NbC have been added to form composite coatings.[13]

To explain the wear resistance mechanism of such laser remelted composite coatings, the influence of the addition of large amounts of refractory carbides, especially WC, on the microstructures of laser remelted NiCrBSi alloy coatings has been profoundly investigated. Wang et al. found that the laser remelting process of the 40-60 wt.% WC+NiCrBSi coatings promoted a multiphase structure, including a NiCrBSi matrix, distributed WC fragments, flower-like WC structures, and the new hard phase existing in the form of humps.[14] Nerz et al. observed that when the amount of WC reached 60 wt.%, the WC might decarburize to form W_2C, depending on time and temperature.[15] However, some research work indicated that although the addition of large amounts of WC could raise the abrasive-wear resistance of laser remelted composite coatings, it was harmful to the components working at wear-corrosion conditions at which the maximum addition of WC should be below 15 wt.%.[16,17] Unfortunately, they did not report the influence of such a small amount of WC on the microstructures of laser remelted WC+NiCrBSi composite coatings.

In the present work, the NiCrBSi alloy coating and the NiCrBSi+10wt.%WC composite alloy coating were laser remelted. The microstructures of both alloy coatings after laser remelting were investigated by using x-ray diffraction (XRD), scanning and transmission electron microscopy (SEM and TEM), as well as microanalysis techniques such as energy dispersion x-ray (EDX) spectrum analysis.

2. Experimental Procedures

The substrate of S45C steel, which is composed of C 0.45, Mn 0.8, and Fe balance (in wt.%), was cut into $8 \times 8 \times 60$ mm^3. The coating powder (Jiujiang Alloy Powder, Ltd., Jiujiang, Jiangxi, P.R. China) for laser surface melting was the self-fluxing NiCrBSi alloy powder with composition of C 1.0, B 4.0, Si 4.0, Fe 12, Cr 17, and Ni the balance (in wt.%); the mean particle size averaged about 85 μm. In addition, WC

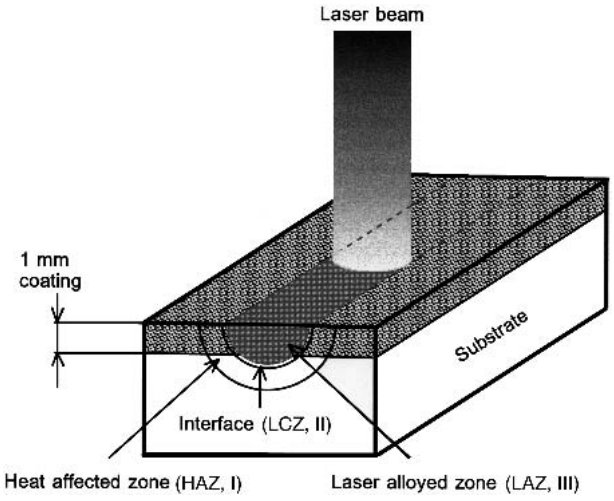

Fig. 1 Schematic diagram of laser irradiation

Y.M. Zhang, M. Hida, A. Sakakibara, and **Y. Takemoto,** The Graduate School of Natural Science and Technology, Okayama University, 3-1-1 Tsushima-naka, Okayama 700-8530, Japan. Contact e-mail: zhangyimin@hotmail.com.

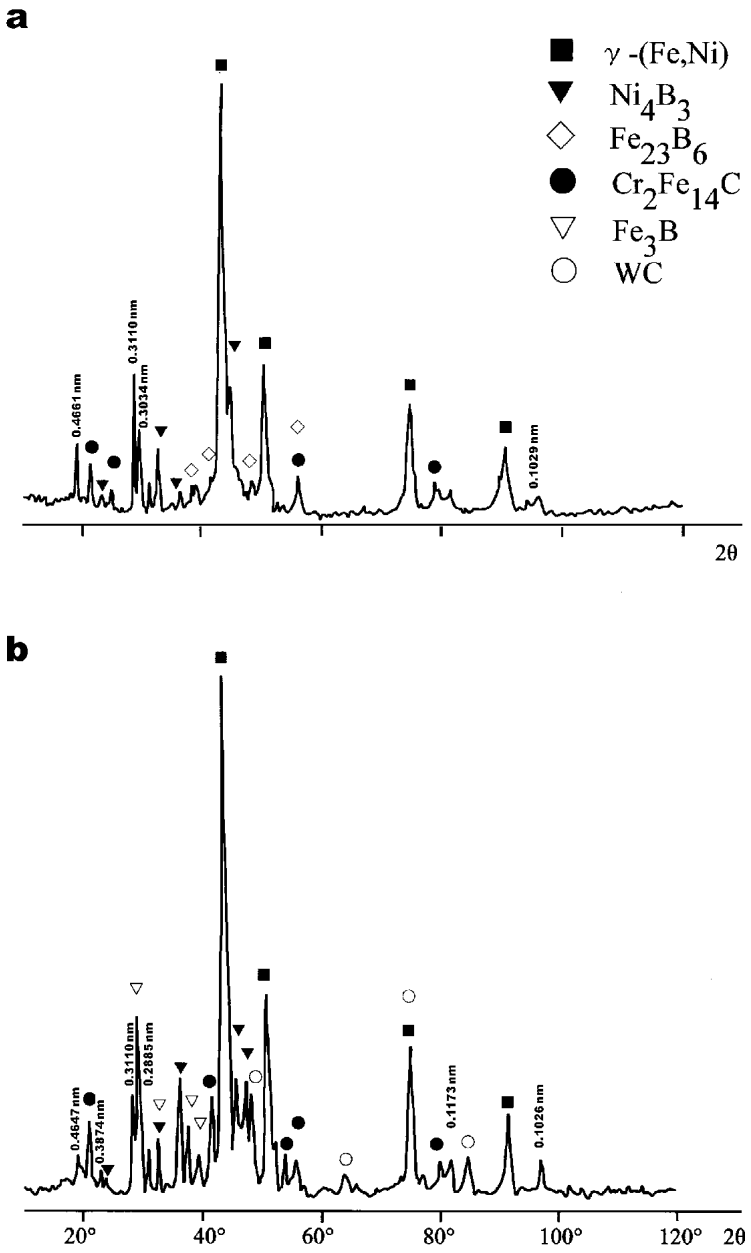

Fig. 2 The XRD results for the two kinds of samples: **(a)** NiCrBSi alloyed layer, **(b)** NiCrBSi+10wt.%WC alloyed layer

powder was mixed to the above powder. Thus, the two kinds of alloy powders used in the experiment were NiCrBSi and NiCrBSi+10wt.%WC. These powders were mixed with 0.05 wt.% rosin in a mortar, and ground together with a small amount of alcohol; then the mixture was overlayed on the surface of the substrate to a thickness of 1.0-1.1 mm.

A 2.0 kW CO_2 Cross-electroexciter laser (Huazhong University of Science and Technology, Wuhan, Hubei, P.R. China) was used to melt the coating powders (Fig. 1). The working parameters were as follows: beam diameter, 6.0 mm; scanning speed, 7.0 mm/s; and off-focus value, 250 mm. The N_2 gas was used to protect the melting pool. Slices with 0.3 mm thickness were cut out normal to the laser beam scanning direction, then thinned mechanically, and Ar ion-milled to the final TEM films.

The XRD was carried out on a PW 1700 (Rigaku Co. Ltd., Tokyo, Japan) x-ray diffractometer with Cu Kα radiation (2θ = 15-120°). The microstructure of the laser melted layer was observed with JSM-35CF (JEOL Ltd., Tokyo, Japan) SEM. The EDX spectrum analysis was made on an EM 002B (Topcon Ltd., Tokyo, Japan) transmission electron microscope. TEM observation was carried out using an EM 002B and a JEM 4000EX (JEOL).

3. Results and Discussion

3.1 X-Ray Diffraction Analysis

Figure 2(a) and (b) shows the XRD patterns of NiCrBSi and NiCrBSi+10 wt.%WC laser alloyed layers, respectively. Table 1

Table 1 The Lattice Type and Parameter of the Two Kinds of Samples

Phase	NiCrBSi	NiCrBSi + WC	Type	A, B, C, nm	α, β, γ
γ-(Fe,Ni)	○	○	FCC	A = 0.3596	
Fe_3B		○	Orthorhombic	A = 0.5428	
				B = 0.6699	
				C = 0.4439	
$Fe_{23}B_6$	○		FCC	A = 1.076	
Ni_4B_3	○	○	Rhombohedral	A = 0.6428	β = 103.3
				B = 0.4879	
				C = 0.7819	
WC		○	Hexagonal	A = 0.2906	
				B = 0.2837	
$Cr_2Fe_{14}C$	○	○	FCC	A = 0.7200	

presents the lattice types and parameters of the phases in both laser alloyed layers. Peaks at interplanar spacing d = 0.4661 nm, 0.3110 nm, 0.3034 nm, and 0.1029 nm for the NiCrBSi sample, and at interplanar spacing d = 0.4647 nm, 0.3874 nm, 0.3110 nm, 0.2885 nm, 0.1173 nm, and 0.1026 nm for the NiCrBSi+10wt.%WC sample were difficult to be indexed. Although some peaks with certain identifications at interplanar spacing, such as d = 0.4661 nm, 0.3110 nm, and 0.2885 nm, were well matched with those of an orthorhombic iron silicon carbide (according to JCPDS, 18-651), some peaks (such as d = 0.3874 nm, 0.3034 nm, 0.1173 nm, and 0.1029 nm) were not as consistent with this phase due to their weak and uncertain identification for laser alloyed layer. Some work was still needed to further clarify it. However, the above XRD results show that the addition of WC has little influence on the intensity and positions of peaks of this iron silicon carbide.

3.2 SEM Observation

Figure 3 shows the cross-sectional microstructures in both alloyed layers, which can be divided into three regions: laser alloyed zone (LAZ), interface, and heat affected zone (HAZ).

It is noted from Fig. 3 that although the typical quenched structure of S45C steel should be a mixed structure of lath and block martensites, a very fine lath martensitic structure has occurred in the heat-affected substrate (about 15 μm in width) of both samples near the interface. This result is the same as in Ref. 18.

The SEM images of the interface in both laser alloyed samples are shown as a smooth bright layer (Fig. 3). This smooth bright layer is the solid/liquid interface in the laser melting and the rapid solidification process. There is a flat interface in the NiCrBSi sample, but the interface is quite rough after the addition of WC, as shown in Fig. 3(a) and (b).

In general, it is thought that at the beginning of solidification, a great positive temperature gradient exists in the liquid side of solid/liquid interface, so the crystals grow in a planar manner on solidification to form the interface.[19-21]

After rapid solidification, LAZ of NiCrBSi is composed of thick primary crystal and polytropic eutectic. From near the interface to the top of the surface, it changes gradually from cellular to dendritic structures (Fig. 3a). It was found in Fig. 3(a) that the growing direction of crystals is disorderly in the initial stage of solidification in LAZ, and some dendritic crystals are vertical to interface, while others are inclined to it.

Figure 3(b) shows the SEM image taken from the NiCrBSi+10wt.%WC laser alloyed layer. Compared with the LAZ of NiCrBSi, the LAZ of NiCrBSi+10wt.%WC presents quite different microstructural features. Instead of the thick dendritic structure in the LAZ of NiCrBSi, the LAZ of NiCrBSi+10wt.%WC is a compound structure of relatively finer dendrite and blocks with different sizes and shapes denoted as 1 and 2 in the LAZ of Fig. 3(b). To determine the structure of the blocks, energy dispersive x-ray spectra (EDS) analyses were carried out. The EDS results taken from one of those blocks give the composition of C13.91, Cr38.71, and W47.37 in wt%. Thus, the blocks are probably the undissolved or partly dissolved WC particles that have a relatively high melting point. In the rapid solidification process, these WC particles, either undissolved or partly dissolved, play a role of nucleating sites and prevent grains from growing, which results in some finer cellular or dendritic structure in the LAZ of NiCrBSi+10wt.%WC. Furthermore, EDS line analyses from substrate to the LAZ in Fig. 3(a) and (b) was performed to determine the composition distribution (Fig. 4). It is found in Fig. 4 that the addition of WC particles has little influence on the composition distributions of elements Ni, Fe, and Si in the vicinity of the interface. On the other hand, the distributions of elements Cr and W have obvious changes, especially the existence of element W in region A of Fig. 3(b). However, it should be noted that in the LAZ of NiCrBSi+10wt.%WC, apart from a very narrow cellular belt, there exists a eutectic zone (region A) about 20-25 μm in width near the interface. In this eutectic zone, no WC blocks can be recognized although EDS line analysis clearly proves the existence of element W.

Using laser processing, the melting pool was severely stirred and even boiled under the radiation of high energy density laser beams, which caused the undissolved or partly dissolved WC particles to be whirled into the inner part of the LAZ of NiCrBSi+10wt.%WC. The already dissolved WC particles provided W and the element W + Fe from the substrate to form a boride structure $(Fe, M)_{XB}$ in the eutectic. This is probably why the EDS line analysis shows the existence of element W, but WC particles cannot be found in region A of Fig. 3(b).

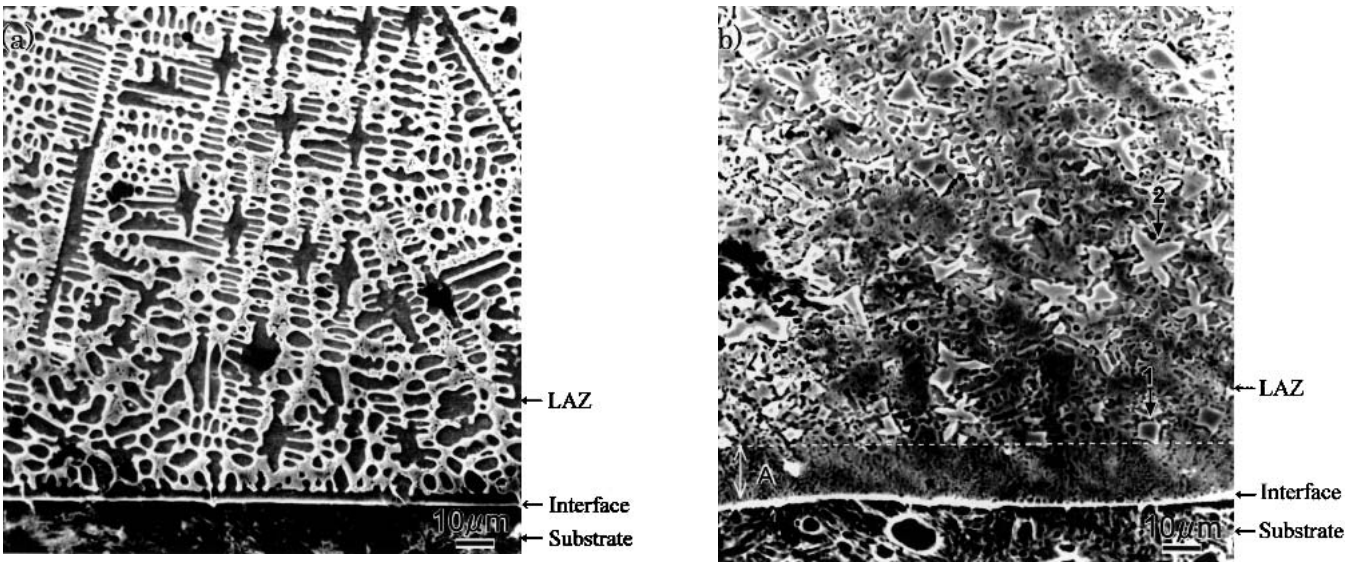

Fig. 3 SEM images for the two kinds of samples: **(a)** NiCrBSi alloyed layer, **(b)** NiCrBSi+10wt.% WC alloyed layer

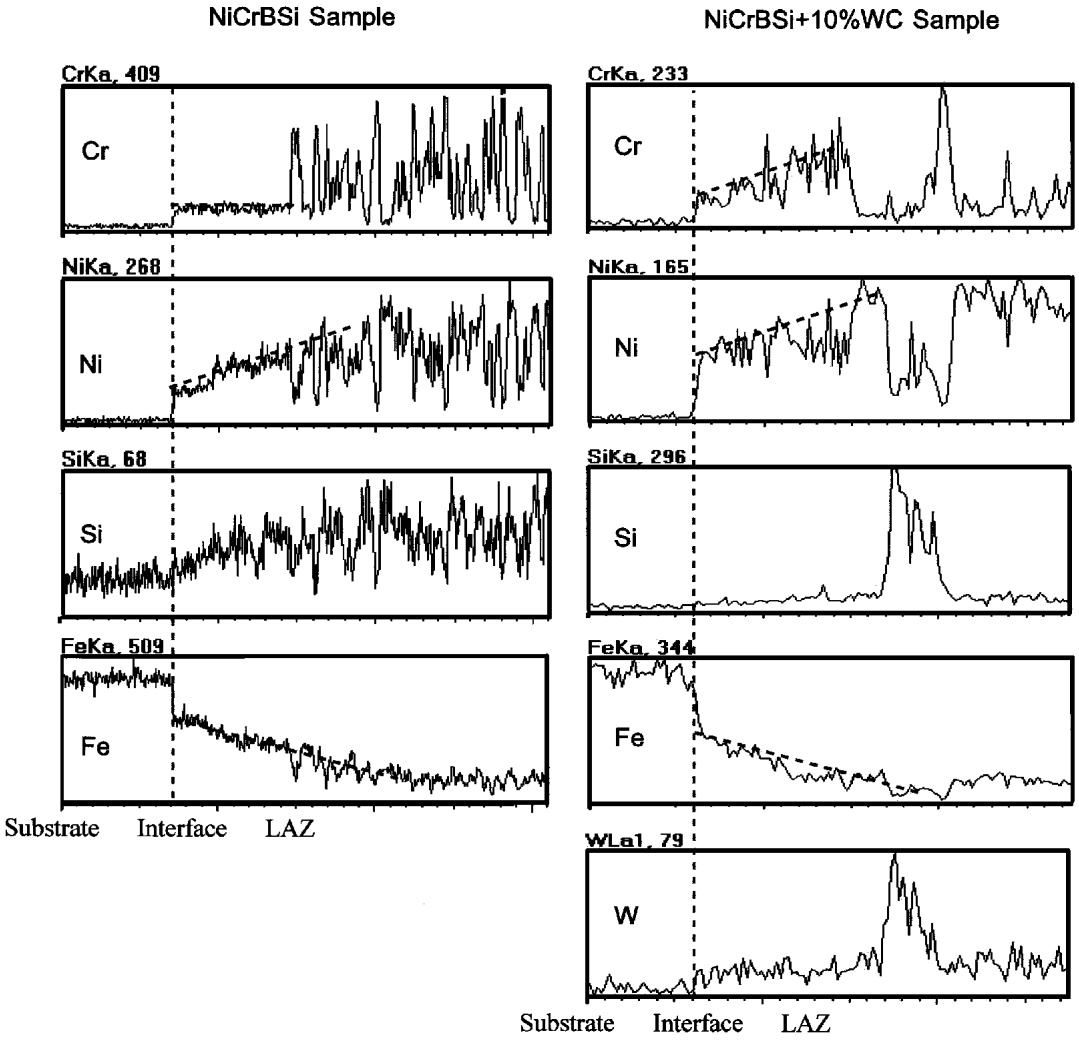

Fig. 4 The results of EDS line analysis from substrate to the region near the top of the melted pool in the two kinds of samples

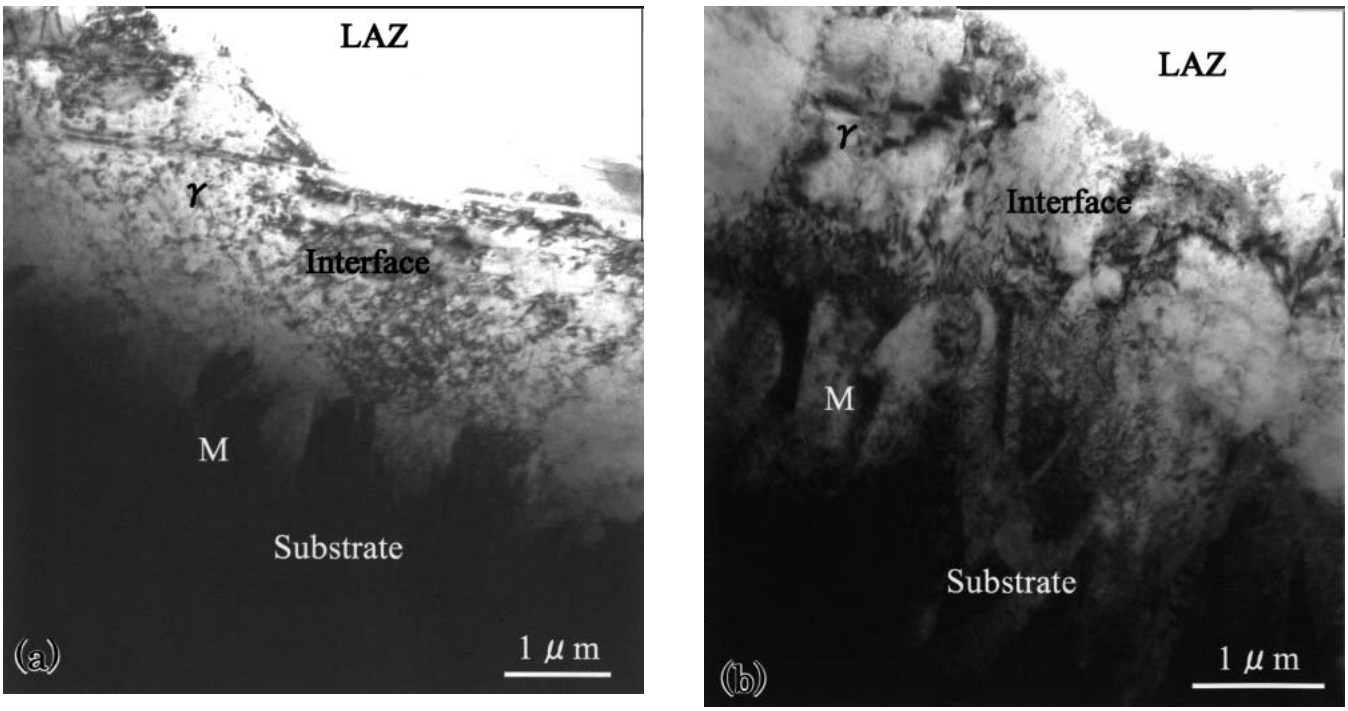

Fig. 5 TEM images in the two kinds of samples: **(a)** NiCrBSi alloyed layer, **(b)** NiCrBSi +10 wt.% WC alloyed layer

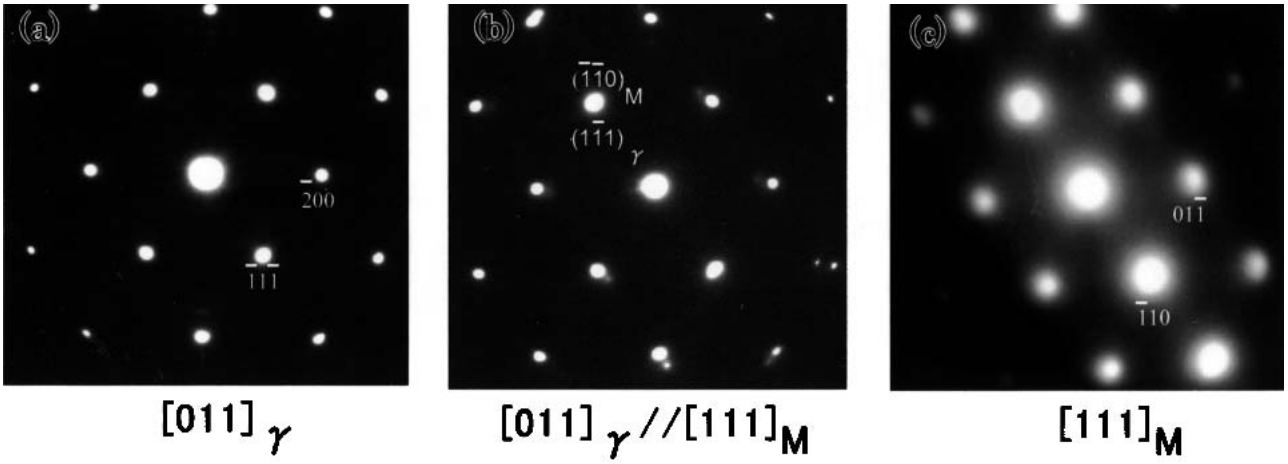

Fig. 6 EDPs and indices including γ-(Fe,Ni) and martensite phases in NiCrBSi sample: **(a)** ED pattern of γ-(Fe, Ni) phase, **(b)** ED pattern including γ-(Fe, Ni) and martensite phases, **(c)** ED pattern of martensite phase

3.3 TEM Observation

3.3.1 Interface Layer. The microstructures in the laser alloyed layer normal to the laser beam scanning direction have been observed via TEM. Figure 5(a) and (b) shows the interface of both samples, respectively. The approximate thickness of the interface is 2.0 μm. The martensite grows in two directions near the interface. Systematic tilt experiments were carried out to obtain a series of electron diffraction patterns (EDPs) to identify the structure of the martensite and interface layer. By EDP analysis and observation in the region about 30 μm wide along the interface, it was found that the interface region in both NiCrBSi and NiCrBSi+10wt.%WC samples consists of a single phase (i.e., super-saturated γ-(Fe, Ni) solid solution). Figure 6 shows a series of EDPs of the NiCrBSi sample and the indices corresponding to γ-(Fe, Ni) phase and martensite. Figure 6(a) shows the EDP of the interface γ-(Fe, Ni) phase along its $[011]_\gamma$ zone axis. The EDP including both γ-(Fe, Ni) phase and martensite is shown in Fig. 6(b). It was found in Fig. 6(b) that $(111)_\gamma$ plane of γ-(Fe, Ni) phase nearly parallels $(110)_M$ of martensite. Figure 6(c) shows that the EDP of martensite is along the $[111]_M$ zone. The $[011]_\gamma$ of γ-(Fe, Ni) phase almost parallels the $[111]_M$ of martensite. Therefore, we obtain the lattice relationship between the martensite and the interface γ-(Fe, Ni) phase as follows:

$$[011]_\gamma // [111]_M$$

$$(111)_\gamma // (110)_M$$

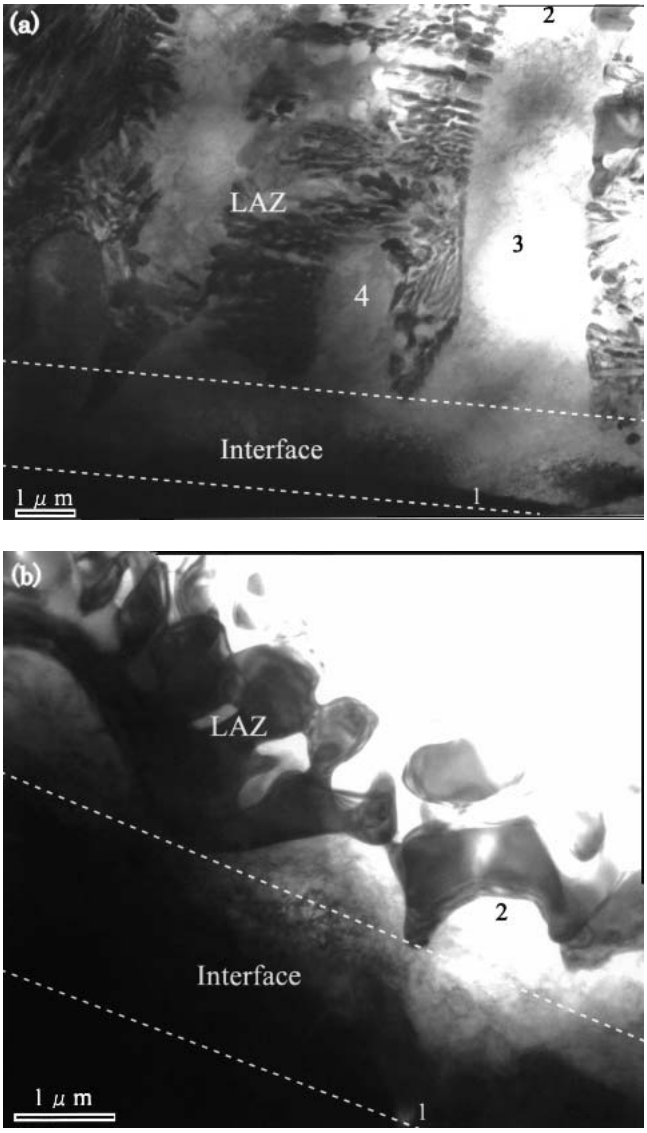

Fig. 7 TEM morphology of laser-alloyed layer in two kinds of samples: **(a)** NiCrBSi alloyed layer, **(b)** NiCrBSi +10 wt.% WC alloyed layer

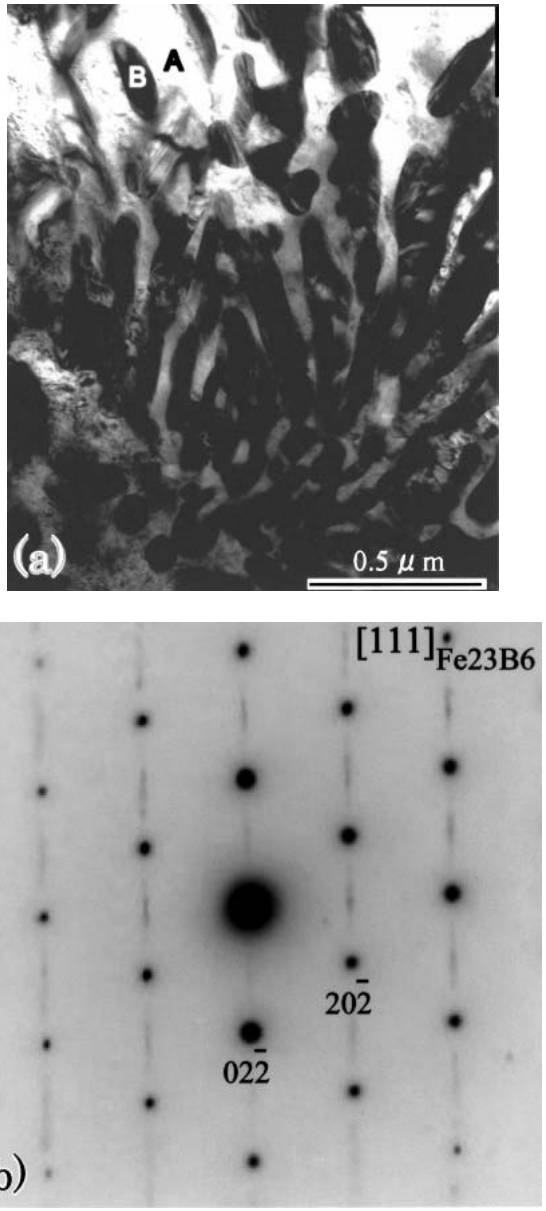

Fig. 8 The eutectic structure in NiCrBSi sample: **(a)** BF image, **(b)** EDP

This relationship corresponds to the typical Kurdjumov-Sachs (K-S) lattice relation in martensite.

3.3.2 Effect of WC on Primary Arms. Figure 7(a) and (b) shows the cellular structures in the two kinds of samples mentioned above, respectively. The interface composed of a single phase γ-(Fe, Ni) is planar, grown along the $[110]_M$ of martensite. The protrusion or primary arms grow in the direction of $[111]_\gamma$ on the planar interface. They develop eventually into long arms or cells from the interface (marked as 3 and 4 in Fig. 7a) along the direction of heat flow. The lengths of the arms and cells (such as 3 and 4 in Fig. 7a) were measured statistically from many images to be about 10.5 μm and 3.0 μm, respectively. The same results have been shown in Fig. 3(a). The compositions from the interface (marked as number 1 in Fig. 7a) to the top of the primary arm (marked as number 2 in Fig.7a) were measured successively. The concentrations of the elements changed from Fe85.60, Ni11.31, Si0.14, and Cr2.95 (in wt.%) at the interface, to Fe59.17, Ni34.97, Si1.41, and Cr4.45 (in wt.%) at the top of the primary arm.

The cellular structures of γ-(Fe, Ni) are shown in Fig. 7(b) after the addition of WC. The protrusion growing on the interface had a cellular structure, and the lengths of the protrusions in Fig. 7(b) statistically measured as 1.0 μm, are shorter than those of the primary arms of 3 and 4 in Fig. 7(a). The compositions from the interface (marked as number 1 in Fig.7b) to the top of the primary arms (marked as number 2 in Fig.7b) were also measured to compare with those of NiCrBSi. The measurements showed that the concentrations of the elements changed from Fe82.48, Ni12.52, Si0.86, and Cr4.14 (in wt.%) at the interface to Fe51.10, Ni38.14, Si1.27, and Cr9.49 (in

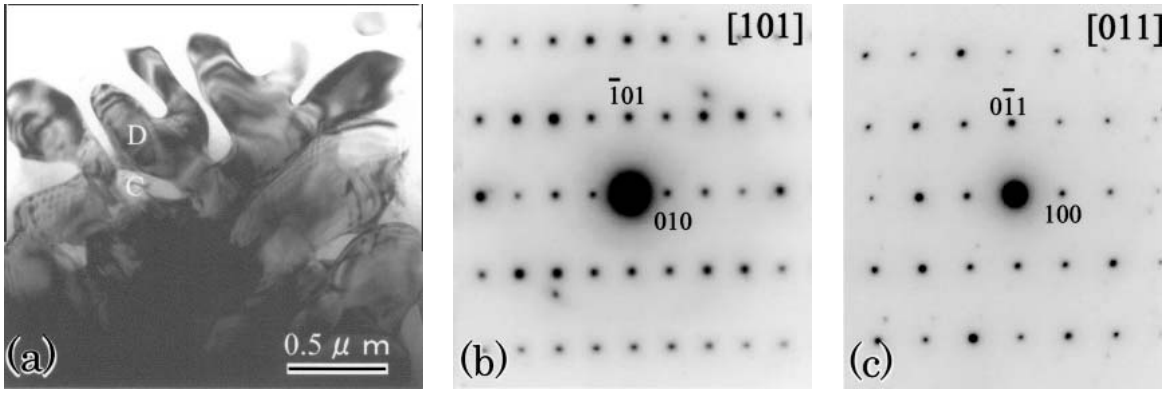

Fig. 9 The eutectic structure in NiCrBSi+10wt.%WC sample: **(a)** BF image, **(b,c)** EDPs of the phase

wt.%) at the top of the primary arm. It is evident that the addition of WC has an influence on the composition distributions of elements, especially the element Cr. In addition, there is no dendrite formation in the region near the interface. It can also be found in Fig. 3(b) that there is only eutectic structure in the range of 20-25 μm away from the interface.

3.3.3 Effect of WC on Eutectic Structure. The TEM image of the eutectic structure and its corresponding EDP in the NiCrBSi sample are shown in Fig. 8. Electron diffraction experiments have proved that the eutectic structure in the NiCrBSi sample consists of γ-(Fe, Ni) solid solution phase (region A of Fig. 8a) and stick-like or rod-like Fe23B6 (region B of Fig. 8a). The EDP and the corresponding index of Fe23B6 are shown in Fig. 8(b). However, the eutectic structure near the interface in the laser melted NiCrBSi+10wt.%WC coating has changed due to the addition of WC. TEM observation and analysis have shown that, besides the γ-(Fe, Ni) solid solution (region C in Fig. 9a) and the boride phase Fe_3B as detected by XRD in Fig. 2(b), certain new phases near the interface (region D in Fig. 9a) formed while the boride $Fe_{23}B_6$ in the eutectic structure of the NiCrBSi sample could not be observed. To determine the structure of this new phase, a set of EDPs were carried out as shown in Fig. 9(b) and (c). It is found that this new phase has an orthorhombic structure with the lattice parameters as: a = 0.554 nm, b = 0.699 nm, and c = 0.458 nm, which are a little larger than those of the boride Fe_3B. The EDS of this new phase gives the composition of Fe 63.04, Ni 22.18, Cr 12.4, W 2.22, and Si 0.16 (in wt.%). Such high content of elements Cr and W suggest that this new phase probably has the structure of $(Fe, Cr, W)_{3B}$. Some detailed investigations are still under way to precisely determine the structure of this phase.

The reason for this structural change of $(Fe, Cr, W)_{3B}$ is probably as follows. Because the melting point of NiCrBSi is relatively lower, more substrates were melted in the laser alloying process and more Fe element came into the melting pool. Then Fe combined with B and formed the Fe23B6 phase. However, the NiCrBSi+10wt.%WC powder has a higher melting point due to the addition of the WC, and less substrate should have been melted. The change in the concentration of elements mentioned in Section 3.3.2 illustrated that relatively less Fe (about 50 wt.%) came into the laser melted pool, and that the already dissolved WC particles provided element W combined with the elements Fe and Cr, thus giving rise to the existence of a $(Fe, Cr, W)_{3B}$ phase in the eutectic structure.

4. Conclusions

1) The laser alloyed layer for two samples is divided into three zones. At the beginning of solidification, the interface grows in a planar fashion with 2 μm in thickness. It is a γ-(Fe, Ni) single solid solution.
2) The relationship between the martensite in the substrate and the interface γ-(Fe, Ni) phase agrees well with the K-S relationship.
3) The laser alloyed zone of NiCrBSi is composed of a long primary crystal oriented to $[111]_\gamma$ and eutectic. After the addition of WC, it presents different structural features. The undissolved or partly dissolved WC particles prevent grains from growing, which results in a fine dendritic structure. Furthermore, a eutectic zone exists near the interface. A certain new boride phase with the structures of $(Fe, Cr, W)_{3B}$ was formed in this eutectic zone.
4) The addition of WC particles has obvious influences on the composition distribution of Cr in the vicinity of the interface. The primary arms have smaller cellular structures on the planar interface.

References

1. H. De Beurs, J.A. Hovius, and J.Th.M. De Hosson: "Enhanced Wear Properties of Steel: A Combination of Ion Implantation Metallurgy and Laser Metallurgy," *Acta Metall.*, 1988, *36*(12), pp. 3123-30.
2. M.J. Hsu and P.A. Molian: "Machining Characteristics of Laser Tungsten Surface-Alloyed M2 High Speed Steel," *Wear*, 1989, *132*, pp. 123-37.
3. H.J. Hegge, H. De Beurs, J. Noordhuis, and J.Th.M. De Hosson: "Tempering of Steel During Laser Treatment," *Metall. Trans. A*, 1990, *21A*, pp. 987-95.
4. B.D. Zhu, X.Y. Zeng, Z.Y. Tao, S.G. Yang, and K. Gui: "Coarse Cemented WC Particle Ceramic-Metal Composite Coatings Produced by Laser Cladding," *Wear*, 1993, *170*, pp. 161-66.
5. D.I. Pantelis, G. Pantazopoulos, and S.S. Antoniou: "Wear Behavior of Anti-Galling Surface Textured Gray Cast Iron Using Pulsed-CO_2 Laser Treatment," *Wear*, 1997, *205*, pp. 178-85.
6. H.J. Niu and I.T.H. Chang: "Microstructural Evolution During Laser

Cladding of M2 High-Speed Steel," *Metall. Mater. Trans. A*, 2000, *31A*(10), pp. 2615-25.
7. Y.M. Zhang, M. Hida, H. Hashimoto, Z.P. Luo, and S.X. Wang: "Effect of Rare-Earth Oxide (CeO_2) on the Microstructures in Laser Melted Layer," *J. Mater.Sci.*, 2000, *35*(21), pp. 5389-5400.
8. L.R. Katipelli, A. Agarwal, and N.B. Dahotre: "Laser Surface Engineered TiC Coating on 6061 Al Alloy: Microstructure and Wear," *Appl. Surf. Sci.*, 2000, *153*(2-3), pp. 65-78.
9. A. Roy and I. Manna: "Laser Surface Engineering to Improve Wear Resistance of Austempered Ductile Iron," *Mater. Sci. Eng., A*, 2001, *A297*(1-2), pp. 85-93.
10. T.M. Yue, J.K. Yu, and H.C. Man: "The Effect of Excimer Laser Surface Treatment on Pitting Corrosion Resistance of 316LS Stainless Steel," *Surf. Coat. Technol.*, 2001, *137*(1), pp. 65-71.
11. W. Xibao, L. Yong, and Y. Songlan: "Formation of TiB_2 Whiskers in Laser Clad Fe-Ti-B Coatings,'' *Surf. Coat. Technol.*, 2001, *137*(2-3), pp. 209-16.
12. N.R. Harlan, R. Reyes, D.L. Bourell, and J.J. Beaman: "Titanium Castings Using Laser-Scanned Data and Selective Laser-Sintered Zirconia Molds," *J. Mater. Eng. Perf.*, 2001, *10*(4), pp. 410-03.
13. W. Ceri, R. Mortinella, G.P. Mor, P. Bianchi, and D.D. Anglo: "Property Analysis for Carbon-Tungsten Alloys Laser Cladding Treatment," *Surf. Coat. Technol.*, 1991, *49*, pp. 40-45.
14. H. Wang, W.M. Xia, and Y.S. Jin: "A Study on Abrasive Resistance of Ni-Based Coatings With a WC Hard Phase," *Wear*, 1996, *195*, pp. 47-52.
15. T.C. Nerz, J.E. Nerz, B.A. Kushner, and W.L. Riggs: "Microstructures Evolution in Laser Clad WC Coatings," *Surf. Eng.*, 1993, *9*, pp. 3-10.
16. B.H. Tian and J.L. Huang: "Effect of Rare-Earth Oxide and Laser Remelting Technique on Wear Resistance of Composite Alloy Flame Spray Coating," *J. Welding*, 1996, *17*, pp. 17-22 (in Chinese).
17. J.L. Huang and S.A. Zheng: "Effect of WC Content on Wear-Corrosion Behaviors of Laser Remelted Coatings," *Heat Working Technol.*, 2000, *21*, pp. 23-29 (in Chinese).
18. S.Y. Zhang and K.Q. Zheng: "Electron Micro-Analysis for C-N-B Laser Alloyed Layer on 60# Steel Surfaces," *Chin. J. Lasers*, 1990, *17*(1), pp. 40-44.
19. D.A. Porter: *Phase Transformation in Metals and Alloys,* Van Nostrand Reinhold Co. Ltd., 1981, pp. 213-15.
20. S. Yang, W.D. Huang, X. Lin, Y.P. Su, and Y.H. Zhou: "Microstructure of Cu-27.3%Mn Alloy Under Laser Rapid Remelting and Solidification Condition," *Acta Metall. Sci.*, 2000, *36*(1), pp. 12-16.
21. C. Caesar: "Undercooling and Crystal Growth Velocity During Rapid Solidification," *Adv. Eng. Mater.*, 1999, *1*(1), pp. 75-79.